Magneto-Hydrodynamics and the Tearing Mode Instability

Vinay Kumar

Email: *vinay.kumar@icts.res.in*

Project Supervisor:

Prof. Pallavi Bhat

International Centre for Theoretical Sciences

Shivakote, Hesaraghatta Hobli, Bengaluru 560089, India.

Contents

Chapter 1

Magneto-Hydrodynamics (MHD)

1.1 Introduction

Magnetic fields are widely encountered in the universe. They play crucial roles in the formation and structure of galaxies, evolution of stars, supernovae bursts, and accretion around quasars and black holes. The reason magnetic fields are ubiquitous is because most of the baryonic matter in the universe is in the form of hot ionized plasma. Moving plasmas constitute electric current and, as a result, host magnetic fields.

To describe the properties and behavior of these plasmas, which can be modeled as fluids, hydrodynamic equations coupled with Maxwell's equations of electromagnetism are used. The study of magnetic fields and associated plasmas in this framework is called magnetohydrodynamics.

1.2 The Equations of MHD

We work in Gaussian cgs units and the Maxwell's equations for the electric field $\boldsymbol{E}$ and the magnetic field $\boldsymbol{B}$, given a current density $\boldsymbol{J}$ and a charge density ρ_e, with this choice of units are:

$$\frac{1}{c}\frac{\partial \boldsymbol{B}}{\partial t} = -\nabla \times \boldsymbol{E}, \quad \nabla \cdot \boldsymbol{B} = 0, \tag{1.1}$$

$$\frac{1}{c}\frac{\partial \boldsymbol{E}}{\partial t} = \nabla \times \boldsymbol{B} - \frac{4\pi}{c}\boldsymbol{J}, \quad \nabla \cdot \boldsymbol{E} = 4\pi\rho_e. \tag{1.2}$$

Also, we work in the Lorenz gauge wherein we define $\boldsymbol{B} = \nabla \times \boldsymbol{A}$ where $\boldsymbol{A}$ is the vector potential. "Uncurling" equation 1.1, we get the dynamic equation for the vector potential as:

$$\frac{1}{c}\frac{\partial \boldsymbol{A}}{\partial t} = -\boldsymbol{E} - \nabla\phi, \tag{1.3}$$

where ϕ is the electric scalar potential.

1.2.1 The Induction Equation

We use the general form of Ohm's Law, $\boldsymbol{J} = \sigma\left(\boldsymbol{E} + \frac{\boldsymbol{V}\times\boldsymbol{B}}{c}\right)$ to substitute for $\boldsymbol{J}$ in equation 1.2, we get:

$$\frac{\eta}{c^2}\frac{\partial \boldsymbol{E}}{\partial t} + \boldsymbol{E} = \frac{\eta}{c}\nabla\times\boldsymbol{B} - \frac{\boldsymbol{V}\times\boldsymbol{B}}{c}. \tag{1.4}$$

Here $\eta = c^2/4\pi\sigma$ is the magnetic diffusivity of the plasma. If the electric field varies over timescales larger than the Faraday timescale, $\tau_F \equiv \frac{\eta}{c^2}$, the first term of the above equation can be neglected. Taking curl of what remains of equation 1.4 and using equation 1.1,

$$\frac{\partial \boldsymbol{B}}{\partial t} = \nabla\times(\boldsymbol{V}\times\boldsymbol{B}) - \eta\nabla\times\nabla\times\boldsymbol{B}. \tag{1.5}$$

This is the famous **Induction Equation** for magnetized plasmas. In the absence of $\boldsymbol{V}$, we see that the induction equation reduces to the diffusion equation - the magnetic field *diffuses* - with a rate determined by η, which is why η is called the diffusivity.

1.2.2 The Momentum Equation

The momentum equation is obtained by appending a term for the Lorentz force to the Navier-Stokes equation. The Lorentz force on a charge moving with a velocity $\boldsymbol{V}$ is given by $\boldsymbol{F}_l = q\left[\boldsymbol{E} + (\boldsymbol{V}\times\boldsymbol{B})/c\right] = \rho_e \mathrm{d}\forall\left[\boldsymbol{E} + (\boldsymbol{V}\times\boldsymbol{B})/c\right]$, where $\mathrm{d}\forall$ is an infinitesimal volume element. So we get the Lorentz force density as

$$\boldsymbol{f}_l = \rho_e\boldsymbol{E} + \frac{\boldsymbol{J}\times\boldsymbol{B}}{c}, \tag{1.6}$$

where $\rho_e\boldsymbol{V}$ has been identified as $\boldsymbol{J}$. Let us consider the ratio of the modulus of the two terms on the R.H.S. of equation 1.6:

$$\frac{|\rho_e\boldsymbol{E}|}{|\boldsymbol{J}/c\times\boldsymbol{B}|} \sim \frac{|(\nabla\cdot\boldsymbol{E})\boldsymbol{E}|}{|\,(\nabla\times\boldsymbol{B})\times\boldsymbol{B}|}. \tag{1.7}$$

Assuming that $\boldsymbol{E}$ and $\boldsymbol{B}$ vary over similar length scales, this ratio is of the order $\dfrac{\boldsymbol{E}^2}{\boldsymbol{B}^2}$. For a highly conducting plasma, for finite $\boldsymbol{J}$, Ohm's law tells us that $\boldsymbol{E} \approx -(\boldsymbol{V}\times\boldsymbol{B})/c$. Which means $\dfrac{\boldsymbol{E}^2}{\boldsymbol{B}^2} \sim \dfrac{\boldsymbol{V}^2}{c^2} \ll 1$ for

non-relativistic plasmas. So the first term in equation 1.6 is negligible in comparison to the second term and we write the Lorentz force as

$$\boldsymbol{f}_l = \frac{\boldsymbol{J} \times \boldsymbol{B}}{c}. \tag{1.8}$$

The full momentum equation for non relativistic plasmas looks like

$$\rho \frac{D\boldsymbol{V}}{Dt} = -\nabla p + \frac{\boldsymbol{J} \times \boldsymbol{B}}{c} + \boldsymbol{f} + \boldsymbol{F}_{\text{visc}}, \tag{1.9}$$

where ρ is the mass density of the plasma, p is the local pressure, $\boldsymbol{F}_{\text{visc}}$ is the force due to viscosity and $\boldsymbol{f}$ is the net body force.

1.2.3 The Continuity Equation

As for all fluids, we have the continuity equation,

$$\frac{\partial \rho}{\partial t} = -\nabla \cdot (\rho \boldsymbol{V}), \tag{1.10}$$

which in the incompressible limit ($\rho =$ constant), reduces to $\nabla \cdot \boldsymbol{V} = 0$. The assumption of incompressibility can be made when the average Mach number, Ma $= \sqrt{\langle \boldsymbol{V}^2 / c_s^2 \rangle}$ is less than around 0.3 [1]. Here c_s is the speed of sound in the medium given by $c_S = \partial p / \partial \rho$, evaluated at constant entropy.

For incompressible plasmas, the momentum equation becomes

$$\frac{D\boldsymbol{V}}{Dt} = -\frac{1}{\rho_0}\nabla p + \frac{\boldsymbol{J} \times \boldsymbol{B}}{c\rho_0} + \boldsymbol{f} + \nu \nabla^2 \boldsymbol{V}. \tag{1.11}$$

Equations 1.5, 1.9 and 1.10 in addition to an energy equation for the internal energy, e, and an equation of state, $p = p(\rho, e)$, comprise the full MHD equations.

1.3 Magnetic Reconnection

Magnetic Reconnection is the breaking and rejoining of magnetic field lines in highly conducting plasmas resulting in a change in the topology of the magnetic fields and a violent conversion of magnetic energy into kinetic and thermal energy of the plasma particles. It is observed across length scales - from laboratories to many astrophysical settings. Reconnection is the driving force behind a variety of processes like solar flares, magnetic storms and disruption of magnetic confinement in fusion reactors.

In this report we look at a simple scenario where magnetic reconnection takes place - the tearing mode instability, first analyzed by Furth, Killeen and Rosenbluth in [2].

Chapter 2

Reduced Magnetohydrodynamics (RMHD)

The model we employ to describe our system is the Reduced Magnetohydrodynamics model. This model applies to situations where there exists a large, almost uniform, magnetic field, $\boldsymbol{B} \sim B_z\hat{\boldsymbol{z}}$, also called the *guide field*. Tokamaks and loops in solar atmosphere are some of the popular instances where such a configuration is seen.

2.1 RMHD Ordering

The magnetic field for this configuration can be written as

$$\boldsymbol{B} = B_z\hat{\boldsymbol{z}} + \boldsymbol{B}_\perp, \tag{2.1}$$

where B_z is the guide field and the component of field perpendicular to the guide field is $\boldsymbol{B}_\perp$. Since the guide field is very large compared to the in-plane field, we have

$$\frac{B_\perp}{B_z} \sim \epsilon \ll 1. \tag{2.2}$$

From here on, we choose units wherein $B_z \sim 1$, and so $B_\perp \sim \epsilon$. The idea is to substitute this ordering into the MHD equations and retain terms up-to first order in ϵ.

In-plane energy equipartition gives

$$\frac{\rho V_\perp^2}{2} \sim \frac{p}{\gamma - 1} \sim \frac{B_\perp^2}{8\pi}. \tag{2.3}$$

Since $B_\perp \sim \epsilon$,

$$\begin{aligned} V_\perp &\sim \epsilon, \\ p &\sim \epsilon^2. \end{aligned} \tag{2.4}$$

Since the pressure term is order ϵ^2, we can ignore in-plane pressure dynamics. Short timescales along the z direction imply force balance and gives us the freedom to choose $V_z = 0$.

Since the variation is much more in-plane than along z-axis, we set

$$\begin{aligned} \nabla_\perp &\sim 1, \\ \partial_z &\sim \epsilon. \end{aligned} \tag{2.5}$$

Since B_z is roughly uniform, we split it as

$$B_z = B_{z0} + \widetilde{B}_z. \tag{2.6}$$

So the pressure balance in z direction gives

$$\frac{\partial p}{\partial z} + \frac{\partial}{\partial z}\left(\frac{B_z^2}{8\pi}\right) = 0, \tag{2.7}$$

$$\implies \frac{\partial p}{\partial z} + \frac{B_{z0}}{4\pi}\frac{\partial \widetilde{B}_z}{\partial z} = 0. \tag{2.8}$$

Now $B_{z0} \sim 1$ and $p \sim \epsilon^2$. This implies $\widetilde{B}_z \sim \epsilon^2$ and we can ignore this term since it is second order in ϵ.

Collecting expressions from above, we get the complete reduced MHD ordering as

$$V_z = 0, \quad V_\perp \sim \epsilon, \tag{2.9}$$

$$\frac{\partial}{\partial z} \sim \epsilon, \quad \nabla_\perp \sim 1, \tag{2.10}$$

$$p \sim \epsilon^2, \quad \widetilde{B}_z \sim \epsilon^2. \tag{2.11}$$

2.2 Derivation of RMHD Equations

We start by defining the magnetic field using a flux function ψ,

$$\boldsymbol{B} \equiv \hat{\boldsymbol{z}} \times \nabla\psi + B_{z0}\hat{\boldsymbol{z}}, \tag{2.12}$$

which in the Lorenz gauge means $\psi = -A_z$ and $\boldsymbol{A}_\perp$ is chosen to be zero. This choice automatically satisfies $\nabla \cdot \boldsymbol{B} = 0$.

Ampere's Law then gives us

$$\frac{4\pi}{c}\boldsymbol{J} = \nabla \times (\hat{\boldsymbol{z}} \times \nabla\psi) \tag{2.13}$$

$$= \hat{\boldsymbol{z}}\nabla^2\psi + \mathcal{O}\left(\epsilon^2\right). \tag{2.14}$$

So we keep only the z component of the current density and neglect the others since they are order ϵ^2.

$$\implies \frac{4\pi}{c}J_z = \nabla^2\psi = \nabla_\perp^2\psi. \tag{2.15}$$

2.2.1 The Induction Equation

Subbing equation 2.12 into the Induction equation, 1.5,we get

$$\frac{\partial \boldsymbol{B}}{\partial t} = \frac{\partial}{\partial t}(\hat{\boldsymbol{z}} \times \nabla\psi) = \nabla \times (\boldsymbol{V} \times \boldsymbol{B}) - \eta\nabla \times \boldsymbol{J}. \tag{2.16}$$

Using $\nabla \times (\alpha\boldsymbol{a}) = \alpha(\nabla \times \boldsymbol{a}) - \boldsymbol{a} \times \nabla\alpha$ in the above equation, we get

$$\nabla \times \frac{\partial}{\partial t}(\psi\hat{\boldsymbol{z}}) = \nabla \times (-\boldsymbol{V} \times \boldsymbol{B}) + \eta\nabla \times \boldsymbol{J}, \tag{2.17}$$

which on uncurling becomes

$$\hat{\boldsymbol{z}}\frac{\partial\psi}{\partial t} = -\boldsymbol{V} \times \boldsymbol{B} + \eta\boldsymbol{J} + \nabla\chi. \tag{2.18}$$

Here, χ appears as a scalar potential on account of uncurling equation 2.17.

Separating equation 2.18 into components parallel and perpendicular to the z-axis, we get

$$\frac{\partial\psi}{\partial t} = -(\boldsymbol{V} \times \boldsymbol{B})_z + \eta J_z + \frac{\partial\chi}{\partial z}, \tag{2.19}$$

$$0 = -(\boldsymbol{V} \times \boldsymbol{B})_\perp + \nabla_\perp\chi. \tag{2.20}$$

Since $V_z = 0$, we have

$$(\boldsymbol{V} \times \boldsymbol{B})_z = \boldsymbol{V}_\perp \times \boldsymbol{B}_\perp, \tag{2.21}$$

$$(\boldsymbol{V} \times \boldsymbol{B})_\perp = B_{z0}\hat{\boldsymbol{z}} \times \boldsymbol{V}_\perp. \tag{2.22}$$

So, from equation 2.20, we have

$$\nabla_\perp \chi = B_{z0}\hat{\boldsymbol{z}} \times \boldsymbol{V}_\perp. \tag{2.23}$$

If we take $\phi = \chi/B_{z0}$, then we can choose $\boldsymbol{V}_\perp = \hat{\boldsymbol{z}} \times \nabla_\perp \phi = \hat{\boldsymbol{z}} \times \nabla\phi$ and ϕ acts as a stream-function. This choice preserves the incompressible continuity equation, $\nabla_\perp \cdot \boldsymbol{V}_\perp = 0$; $V_z = 0$. This gives us

$$\frac{\partial \psi}{\partial t} = -(\boldsymbol{V}_\perp \times \boldsymbol{B}_\perp) + \eta J_z + \frac{\partial \chi}{\partial z}, \tag{2.24}$$

$$\implies \frac{\partial \psi}{\partial t} = -\left[(\hat{\boldsymbol{z}} \times \nabla\phi) \times (\hat{\boldsymbol{z}} \times \nabla\psi)\right] + \eta J_z + B_{z0}\frac{\partial \phi}{\partial z}, \tag{2.25}$$

$$\implies \frac{\partial \psi}{\partial t} + (\nabla\phi \times \nabla\psi) \cdot \hat{\boldsymbol{z}} = \eta J_z + B_{z0}\frac{\partial \phi}{\partial z}, \tag{2.26}$$

$$\implies \frac{\partial \psi}{\partial t} + \{\phi, \psi\} = \eta J_z + B_{z0}\frac{\partial \phi}{\partial z}, \tag{2.27}$$

$$\implies \frac{\partial \psi}{\partial t} + \{\phi, \psi\} = \eta J_z. \tag{2.28}$$

Equation 2.28 is the reduced induction equation. Here curly brackets act as Poisson Brackets defined as $\{\phi, \psi\} \equiv \partial_x\phi\partial_y\psi - \partial_y\phi\partial_x\psi$.

2.2.2 The Momentum Equation

The momentum equation, in the absence of pressure dynamics and viscosity is just

$$\rho_0 \left[\frac{\partial \boldsymbol{V}}{\partial t} + \boldsymbol{V} \cdot \nabla \boldsymbol{V}\right] = \frac{\boldsymbol{J} \times \boldsymbol{B}}{c}. \tag{2.29}$$

Taking the z-component of the curl of the above equation, we get

$$\rho_0 \left[\frac{\partial \omega_z}{\partial t} + (\nabla \times (\boldsymbol{V} \cdot \nabla \boldsymbol{V})) \cdot \hat{\boldsymbol{z}}\right] = \left(\nabla \times \left(\frac{\boldsymbol{J} \times \boldsymbol{B}}{c}\right)\right) \cdot \hat{\boldsymbol{z}}, \tag{2.30}$$

where $\omega \equiv \nabla \times \boldsymbol{V}$. Now consider the second term on the left hand side of the above equation,

$$\begin{aligned} \nabla \times (\boldsymbol{V} \cdot \nabla \boldsymbol{V}) &= -\nabla \times (\boldsymbol{V} \times \boldsymbol{\omega}) + \nabla \times \nabla\left(\frac{\boldsymbol{V}^2}{2}\right) \\ &= -\boldsymbol{V}\left(\nabla \cdot \boldsymbol{\omega}\right) - \boldsymbol{\omega} \cdot \nabla \boldsymbol{V} + \boldsymbol{V} \cdot \nabla \boldsymbol{\omega} + \boldsymbol{\omega}\left(\nabla \cdot \boldsymbol{V}\right), \end{aligned} \tag{2.31}$$

where we have used $\nabla \times \nabla\left(\frac{\boldsymbol{V}^2}{2}\right) = 0$,since curl of a gradient is zero.

Taking the z component of equation 2.31 and using $V_z = 0$, and $\nabla \cdot \boldsymbol{V} = 0$,

$$(\nabla \times (\boldsymbol{V} \cdot \nabla \boldsymbol{V})) \cdot \hat{\boldsymbol{z}} = \boldsymbol{V} \cdot \nabla \omega_z, \tag{2.32}$$

$$= (\hat{\boldsymbol{z}} \times \nabla \phi) \cdot \nabla \omega_z, \tag{2.33}$$

$$= (\nabla \phi \times \nabla \omega_z) \cdot \hat{\boldsymbol{z}}, \tag{2.34}$$

$$= \{\phi, \omega_z\}. \tag{2.35}$$

Now $\omega_z = \hat{\boldsymbol{z}} \cdot (\nabla \times (\hat{\boldsymbol{z}} \times \nabla \phi)) = \nabla^2 \phi - \hat{\boldsymbol{z}} \cdot \dfrac{\partial}{\partial z} \nabla \phi = \nabla^2 \phi = \nabla_\perp^2 \phi$ because $\dfrac{\partial}{\partial z} \nabla \phi \sim \mathcal{O}\left(\epsilon^2\right)$.

Coming to the right hand side of equation 2.30,

$$\left(\nabla \times \left(\frac{\boldsymbol{J} \times \boldsymbol{B}}{c}\right)\right) \cdot \hat{\boldsymbol{z}} = \frac{1}{c} \left(\boldsymbol{J} \left(\nabla \cdot \boldsymbol{B}\right) - \boldsymbol{B} \left(\nabla \cdot \boldsymbol{J}\right) + \boldsymbol{B} \cdot \nabla \boldsymbol{J} - \boldsymbol{J} \cdot \nabla \boldsymbol{B}\right) \cdot \hat{\boldsymbol{z}}. \tag{2.36}$$

In this, $\nabla \cdot \boldsymbol{B} = 0$ from Gauss' law, $\nabla \cdot \boldsymbol{J} = \nabla \cdot (\nabla \times \boldsymbol{B}) = 0$ since it the divergence of a curl and $(\boldsymbol{J} \cdot \nabla \boldsymbol{B}) \cdot \hat{\boldsymbol{z}} = \boldsymbol{J} \cdot \nabla B_{z0} = 0$.

$$\implies \left(\nabla \times \left(\frac{\boldsymbol{J} \times \boldsymbol{B}}{c}\right)\right) \cdot \hat{\boldsymbol{z}} = \frac{1}{c} \boldsymbol{B} \cdot \nabla J_z \tag{2.37}$$

$$= \frac{1}{c} \left(B_{z0} \frac{\partial}{\partial z} J_z + (\hat{\boldsymbol{z}} \times \nabla \psi) \cdot \nabla J_z\right) \tag{2.38}$$

$$= \frac{1}{c} \{\psi, J_z\}. \tag{2.39}$$

Subbing all this into 2.30, we get the momentum equation,

$$\rho_0 \left(\frac{\partial \omega_z}{\partial t} + \{\phi, \omega_z\}\right) = \frac{1}{c} \{\psi, J_z\}. \tag{2.40}$$

2.3 RMHD Normalizations

The equations of RMHD as derived above are

$$\frac{\partial \psi}{\partial t} + \{\phi, \psi\} = \eta J_z, \tag{2.41}$$

$$\rho_0 \left(\frac{\partial \omega_z}{\partial t} + \{\phi, \omega_z\}\right) = \frac{1}{c} \{\psi, J_z\}, \tag{2.42}$$

$$\frac{4\pi}{c} J_z = \nabla_\perp^2 \psi, \tag{2.43}$$

$$\omega_z = \nabla_\perp^2 \phi. \tag{2.44}$$

We normalize these equations using a typical length perpendicular to the z-axis, $L_\perp$, a typical magnetic field, B_0, and the Aflvénic velocity, $v_A = B_0/\sqrt{4\pi\rho}$. This leads to the following redefinitions

$$\psi \to \frac{\psi}{L_\perp B_0}, \qquad \phi \to \frac{\phi}{L_\perp v_A}, \tag{2.45}$$

$$J_z \to \frac{4\pi L_\perp}{cB_0} J_z, \qquad \omega_z \to \frac{L_\perp}{v_A}\omega_z, \tag{2.46}$$

$$\eta \to \frac{\eta}{L_\perp v_A} = S^{-1}. \tag{2.47}$$

Here S is called the Lundquist number. With these normalizations, the RMHD equations become

$$\frac{\partial \psi}{\partial t} + \{\phi, \psi\} = \eta \nabla_\perp^2 \psi, \tag{2.48}$$

$$\frac{\partial}{\partial t}\nabla_\perp^2 \phi + \left\{\phi, \nabla_\perp^2 \phi\right\} = \left\{\psi, \nabla_\perp^2 \psi\right\}. \tag{2.49}$$

Chapter 3

Tearing Mode Instability

3.1 Initial Configuration

The initial configuration which develops a tearing mode consists of an inviscid highly conducting plasma with an equilibrium magnetic field which undergoes a sharp reversal across an interface, as shown in figure 3.1.

We choose an equilibrium $\psi_0(x)$ such that $\boldsymbol{B}_0 = \partial_x \psi_0 \hat{\boldsymbol{y}}$ is an odd function. This automatically implies that there exists a current sheet at the interface. Initially, the plasma is assumed to be stationery. Small perturbations are introduced over this equilibrium field such that $\psi(x, y, t) = \psi_0(x) + \psi_1(x) \exp(iky + \gamma t)$ and their growth is studied. ψ_1 is assumed to be an even function in x throughout this analysis.

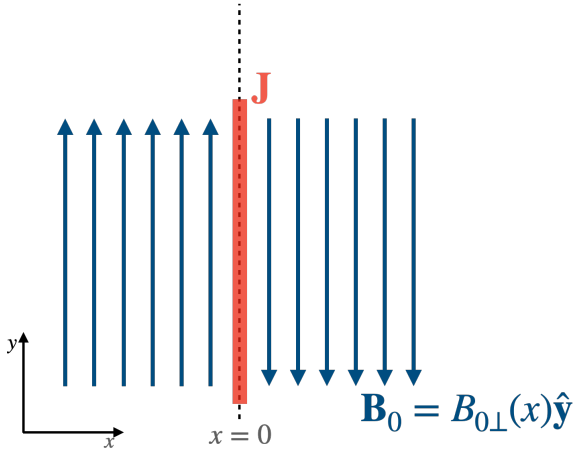

Figure 3.1: Initial configuration for tearing mode instability.

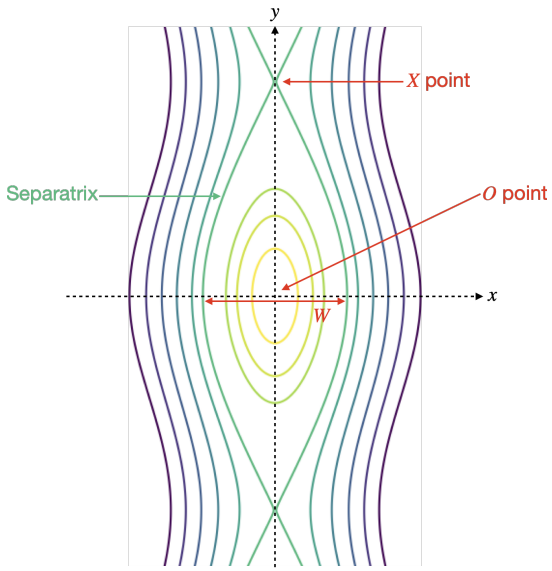

Figure 3.2: Contour plot of $\psi(x, y, t) = \psi_0(x) + \psi_1(x) \exp(iky + \gamma t)$.

This form of ψ corresponds to island shaped contours of ψ, as shown in Figure 3.2. The O-point is at the Origin and the X-points are on the y-axis at $y = \pm\pi/k$. Since $\boldsymbol{B} = \nabla \times \boldsymbol{A}$, the magnetic field in terms of ψ can be written as $\boldsymbol{B} = \partial_x \psi \hat{\boldsymbol{y}} - \partial_y \psi \hat{\boldsymbol{x}}$, which means that lines of constant ψ are also the magnetic field lines.

As we move forward in time, for $\gamma > 0$, the relative amplitude of the perturbations increases. Growing perturbations correspond to an effective "pinching" of field lines at the X-points which subsequently reconnect and form magnetic islands. The contour line passing through the X-points separates the reconnected magnetic islands from the non-reconnected field lines and is hence called the separatrix. The island width, W, is defined as the distance between the x-intercepts of the separatrix.

3.2 FKR Theory

The linear growth stage of the tearing mode instability was first analyzed by Furth, Killeen and Rosenbluth [2].

The initial in-plane equilibrium magnetic field is taken to be of the form $\boldsymbol{B}_0 = B_{\perp 0} f(x) \hat{\boldsymbol{y}}$, where $f(x)$ is taken to be an odd function so that the magnetic field changes direction across the y-axis. Consequently, $f(0) = 0$. The corresponding flux function is ψ_0. Also, at $t = 0$, $\phi_0 = 0$, which implies that the plasma is stationary. We perturb the equilibrium such that the perturbed quantities have the form $\zeta(x, y, t) = \zeta_0(x) + \zeta_1(x) \exp(iky + \gamma t)$ where $\zeta \in \{\psi, \phi\}$.

The RMHD equations (equations 2.48 and 2.49) are linearized and the perturbed quantities ψ and ϕ are

substituted into them. We thus obtain

$$\gamma\left(\partial_x^2 - k^2\right)\phi_1 = ikB_{\perp 0}\left[\left(\partial_x^2 - k^2\right)f\left(x\right) - f''\left(x\right)\right]\psi_1, \tag{3.1}$$

$$\gamma\psi_1 - kB_{\perp 0}f\left(x\right)\phi_1 = \eta\left(\partial_x^2 - k^2\right)\psi_1. \tag{3.2}$$

We define the timescales in the problem

$$\tau_H = \frac{1}{kL_\perp B_{\perp 0}}, \tag{3.3}$$

$$\tau_\eta = \frac{L_\perp^2}{\eta}, \tag{3.4}$$

and rescale ϕ such that

$$\phi_1 \rightarrow -i\gamma\tau_H\phi_1. \tag{3.5}$$

This reduces equations 3.1 and 3.2 to

$$\gamma^2\tau_H^2 L_\perp\left(\partial_x^2 - k^2\right)\phi_1 = \left[f''\left(x\right) - f\left(x\right)\left(\partial_x^2 - k^2\right)\right]\psi_1, \tag{3.6}$$

$$\psi_1 - \frac{f\left(x\right)}{L_\perp}\phi_1 = \frac{L_\perp^2}{\gamma\tau_\eta}\left(\partial_x^2 - k^2\right)\psi_1. \tag{3.7}$$

Solving these equations for ψ_1, ϕ_1 and γ as functions of $f\left(x\right)$, k, with regard to the respective timescales in the system, subject to appropriate boundary conditions, tells us how fast the tearing mode instability grows and what the growing eigenmode is. We make the following assumptions:

1. The instability grows on a hybrid timescale, much shorter than τ_η but much larger that τ_H ($\tau_H \ll 1/\gamma \ll \tau_\eta$).
2. There exists a narrow region, ($x \in [-l_\eta/2, l_\eta/2]$) inside the current sheet where resistive effects come into picture. This width of this region, $l_\eta \ll L_\perp$, is set by the resistivity, η.

With these two assumptions, we use boundary layer theory to find the complete solution of equations 3.1 and 3.2. The domain of interest is separated into three different regions:

- An Inner Region - $|x| < l_\eta/2$ - where resistivity is important, gradients are large, $\partial_x \gg k$, and $f\left(x\right) \sim x$.
- An Outer Region - $|x| \gg l_\eta$ - where resistivity and inertia are negligible.
- An Overlap Region - $l_\eta \ll |x| \ll L_\perp$ - where assumptions of both, the inner and the outer regions apply and the solutions obtained for the inner and outer regions are matched.

3.2.1 The Outer Region

Since inertia and resistivity are negligible, the L.H.S. of equation 3.1 and the R.H.S. of equation 3.2 are very small. So these equations reduce to

$$0 = \left[f''(x) - f(x)\left(\partial_x^2 - k^2\right)\right]\psi_1 \implies \partial_x^2\psi_1 - \left(k^2 + \frac{f''}{f}\right)\psi_1 = 0, \tag{3.8}$$

$$\psi_1 - \frac{f(x)}{L_\perp}\phi_1 = 0 \implies \phi_1 = \frac{L_\perp}{f}\psi_1. \tag{3.9}$$

For a given k and a given form of $f(x)$, these equations can be solved with appropriate boundary conditions,

$$\psi_1 \to 0 \text{ as } x \to \pm\infty, \tag{3.10}$$

and, consequently, ψ_1 and ϕ_1 can be determined in the outer region.

3.2.2 The Overlap Region

For small x, since $f(x)$ is odd, we can use $f(x) \sim x$. Equation 3.8 is still valid and reduces to

$$\partial_x^2\psi_1 = 0, \tag{3.11}$$

since $f''(x) = 0$. Considering the fact that ψ_1 is an even function, the above equation has a solution of the form

$$\psi_1 = \alpha + \frac{|x|}{L_\perp}\beta, \tag{3.12}$$

where α and β are arbitrary constants. It follows from this form that $\partial_x\psi_1\Big|_{0^+} \neq \partial_x\psi_1\Big|_{0^-}$, i.e., $\partial_x\psi_1$ is discontinuous across the current sheet. We define a parameter,

$$\Delta' = \left[\frac{\partial_x\psi_1}{\psi_1}\right]_{0^-}^{0^+} = \left[\partial_x\left(\ln\psi_1\right)\right]_{0^-}^{0^+}, \tag{3.13}$$

which serves as a measure of this discontinuity. Subbing equation 3.12 into the above,

$$\Delta' = \frac{2}{L_\perp}\frac{\beta}{\alpha}. \tag{3.14}$$

From equation 3.8, it is clear that Δ' depends on k and the form of $f(x)$ - it characterizes a particular wavenumber for a particular initial magnetic field configuration and is hence called the *instability pa-*

rameter. Further, it will be seen that Δ' determines whether the perturbations grow or not - whether our configuration is unstable or not.

Now, to determine ϕ_1, we substitute $f \sim x$ in equation 3.9 to obtain

$$\phi_1 = \frac{L_\perp}{x}\psi_1. \tag{3.15}$$

3.2.3 The Inner Region

We now solve equations 3.6 and 3.7 taking $\partial_x \gg k$ and $f(x) \sim x$, without neglecting inertia and resistivity. The equations take the form

$$\gamma^2\tau_H^2 L_\perp \partial_x^2\phi_1 = -x\partial_x^2\psi_1 \implies \partial_x^2\psi_1 = -\gamma^2\tau_H^2\frac{L_\perp}{x}\partial_x^2\phi_1, \tag{3.16}$$

$$\psi_1 - \frac{x}{L_\perp}\phi_1 = \frac{L_\perp^2}{\gamma\tau_\eta}\partial_x^2\psi_1 \implies \partial_x^2\psi_1 = \frac{\gamma\tau_\eta}{L_\perp^2}\left(\psi_1 - \frac{x}{L_\perp}\phi_1\right). \tag{3.17}$$

The variation in ψ_1 in this region, $\delta\psi_1 \sim \dfrac{\mathrm{d}\psi_1}{\mathrm{d}x}l_\eta \sim \psi_1\Delta' l_\eta$, is negligibly small compared to ψ_1 if $\Delta' l_\eta \ll 1$, in which case ψ_1 can be assumed to be constant in the inner region. However, it must be noted that $\partial_x^2\psi_1 \neq 0$ because $\partial_x\psi$ is not constant in the region. Under this assumption, termed the constant-ψ approximation, $\psi_1(x : -l_\eta/2 < x < l_\eta/2) = \psi_1(0)$. Another way to justify the constant-ψ approximation is that being an even function, ψ_1 attains a local extrema at $x = 0$. As a result, $\partial_x\psi_1 \approx 0$ inside the inner region but $\partial_x^2\psi_1 \neq 0$. With this assumption, equation 3.17 reduces to

$$\frac{\gamma\tau_\eta}{L_\perp^2}\left(\psi_1(0) - \frac{x}{L_\perp}\phi_1\right) = \partial_x^2\psi_1. \tag{3.18}$$

Substituting this in equation 3.16, we get

$$\frac{\gamma\tau_\eta}{L_\perp^2}\left(\psi_1(0) - \frac{x}{L_\perp}\phi_1\right) = -\gamma^2\tau_H^2\frac{L_\perp}{x}\partial_x^2\phi_1, \tag{3.19}$$

$$\implies L_\perp^2\partial_x^2\phi_1 = -\frac{\tau_\eta}{\gamma\tau_H^2}\left(\frac{x}{L_\perp}\psi_1(0) - \left(\frac{x}{L_\perp}\right)^2\phi_1\right). \tag{3.20}$$

Equation 3.20 is of the form

$$\chi'' - w^2\chi = w, \tag{3.21}$$

where

$$\chi = -\frac{\phi_1}{\psi_1(0)}\left(\frac{\gamma\tau_H^2}{\tau_\eta}\right)^{1/4}, \tag{3.22}$$

$$w = \frac{x}{L_\perp}\left(\frac{\gamma\tau_H^2}{\tau_\eta}\right)^{-1/4}. \tag{3.23}$$

The solution to 3.21 is given by

$$\chi = -\frac{w}{2}\int_0^1 \mathrm{d}x\,(1-x^2)^{-1/4}\exp\left(-\frac{xw^2}{2}\right). \tag{3.24}$$

Also, integrating equation 3.16 over the inner region, we have

$$-\gamma^2\tau_H^2 L_\perp \int_{-x}^{+x} \mathrm{d}x \frac{\partial_x^2\phi_1}{x} = \int_{-x}^{+x} \mathrm{d}x\partial_x^2\psi_1 \tag{3.25}$$

$$= \partial_x\psi_1\Big|_{+x} - \partial_x\psi_1\Big|_{-x} \tag{3.26}$$

$$= \psi_1(0)\,\Delta' \tag{3.27}$$

Substituting equations 3.22, 3.23 and 3.24 into this, we get

$$\frac{\psi_1(0)}{L_\perp}\gamma^{5/4}\tau_H^{1/2}\tau_\eta^{3/4}\int_{-w}^{+w}\mathrm{d}w\frac{\chi''}{w} = \psi_1(0)\,\Delta'. \tag{3.28}$$

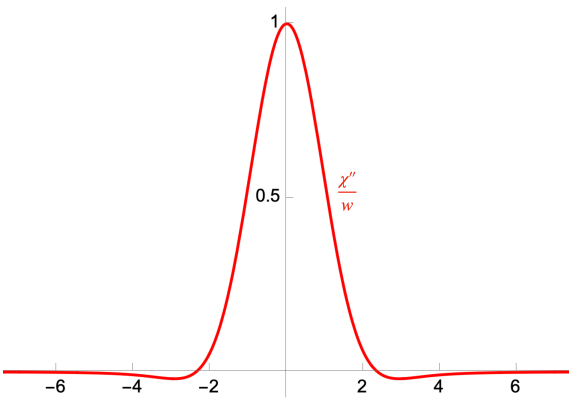

Figure 3.3: Plot of the integrand in equation 3.28.

It can be seen from figure 3.3 that the integrand of the above equation drops to zero as $|w| \to 2$, and so the limits of the integral can be extended to infinity if the width of the tearing layer is such that $|w| \approx 2$. Subbing $w = 2$ and $x = l_\eta$ in equation 3.23, we see that the width of the tearing layer can be approximated

by

$$l_\eta = 2L_\perp \left(\frac{\gamma \tau_H^2}{\tau_\eta}\right)^{1/4}. \tag{3.29}$$

Now, the integral in equation 3.28 is

$$\int_{-\infty}^{\infty} \mathrm{d}w \frac{\chi''}{w} = \frac{4\sqrt{2}}{3}\Gamma\left(3/4\right)\Gamma\left(7/4\right) \approx 2.122, \tag{3.30}$$

using which

$$\gamma \approx 0.55 \left(\Delta' L_\perp\right)^{4/5} \tau_H^{-2/5} \tau_\eta^{-3/5}, \tag{3.31}$$

$$\implies \gamma \approx 0.55 \left(\Delta'\right)^{4/5} \left(kB_{\perp 0}\right)^{2/5} \eta^{3/5}, \tag{3.32}$$

and

$$l_\eta \approx 1.72 L_\perp \left(\Delta' L_\perp\right)^{1/5} \tau_H^{2/5} \tau_\eta^{-2/5}, \tag{3.33}$$

$$\implies l_\eta \approx 1.72 \left(\Delta'\right)^{1/5} \eta^{2/5} \left(kB_{\perp 0}\right)^{-2/5}. \tag{3.34}$$

Non-constant-ψ

We had assumed that the variation in ψ within the tearing layer was negligible. This was under the condition $\Delta' l_\eta \ll 1$. This condition, however, does not hold for large values of Δ', in which case we obtain different scaling laws. The relation between γ and Δ', termed as the dispersion relation, in its full generality is

$$\gamma = \left(\Delta' L_\perp\right)^{4/5} \left(kL_\perp B_{\perp 0}\right)^{2/5} \left(\frac{\eta}{L_\perp^2}\right)^{3/5} \left(-\frac{\pi}{8} u\left[\lambda\left(k\right)\right]\right)^{-4/5}, \tag{3.35}$$

where

$$u\left[\lambda\left(k\right)\right] \equiv \frac{\Gamma\left[\dfrac{\lambda^{3/2}-1}{4}\right]}{\Gamma\left[\dfrac{\lambda^{3/2}+5}{4}\right]}, \qquad \lambda\left(k\right) = \gamma \left(\frac{L_\perp^2}{\eta}\right)^{1/3} \left(kL_\perp B_{\perp 0}\right)^{-2/3}. \tag{3.36}$$

A sample plot of the dispersion relation 3.35 is shown in figure 3.4. For low values of Δ', FKR scaling, (3.32), is recovered and for large values of Δ', we get scaling laws which are like that of the resistive internal kink mode, first derived by Coppi *et al.* [3]:

$$\gamma = \tau_H^{-2/3} \tau_\eta^{-1/3} \tag{3.37}$$

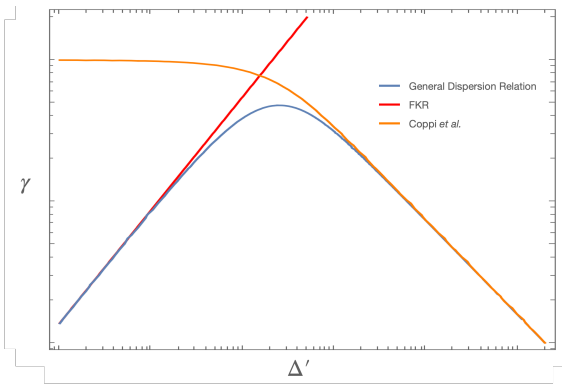

Figure 3.4: Plot of the tearing mode dispersion relation, γ vs Δ', along with FKR and Coppi scaling laws.

3.3 Non-linear Regime

Following the linear growth stage, where the growth of ψ_1 is exponential in time, a non-linear growth stage is seen, where ψ grows algebraically. This happens when the perturbations are sizable compared to the equilibrium fields, and lead to non-negligible second-order eddy currents which oppose linear growth. These eddy currents arise because $B_x = -\partial_y \psi$ is a function of y with non-zero curl. These eddy currents, in turn, lead to Lorentz forces which lead to slowdown of the growth. This non-linear regime was first studied by Rutherford in [4] and is called the Rutherford Regime.

Chapter 4

Simulations using Pencil-Code

Simulations for observing the tearing mode instability were performed using an open source code - the Pencil-Code [5] - available at `https://github.com/pencil-code/`.

Pencil-Code is a high-order finite-difference code for compressible hydrodynamic flows with magnetic fields. It is highly modular and can easily be adapted to different types of problems. The code runs efficiently under MPI on massively parallel shared- or distributed-memory computers. It has been used to simulate many different phenomena - Turbulent Plasmas, Accretion Discs, Dynamos *etc.*

4.1 The Equations of Pencil-Code

The following equations are evolved by Pencil-Code using a third order Runge-Kutta scheme.

The Continuity Equation:

It solves the continuity equation in terms of $\ln \rho$:

$$\frac{\mathrm{D} \ln \rho}{\mathrm{D}t} = -\nabla \cdot \boldsymbol{V}, \tag{4.1}$$

where ρ is the density, $\boldsymbol{V}$ is the fluid velocity, t is time and $\dfrac{\mathrm{D}}{\mathrm{D}t} \equiv \partial_t + \boldsymbol{V} \cdot \nabla$ is the Lagrangian derivative.

The Induction Equation:

Pencil-Code evolves the vector potentials instead of the magnetic fields. For this, it uses the uncurled form of the Induction Equation:

$$\frac{\partial \boldsymbol{A}}{\partial t} = \boldsymbol{V} \times (\nabla \times \boldsymbol{A}) - \eta \nabla \times \nabla \times \boldsymbol{A}, \tag{4.2}$$

where $\boldsymbol{A}$ is the vector potential and η is the magnetic diffusivity of the plasma.

The Equation of State:

We assume an isothermal equation of state,

$$p = \rho c_s^2 \tag{4.3}$$

The Momentum Equation:

The standard momentum equation with the addition of the Lorentz force term is solved

$$\rho \frac{\mathrm{D}\boldsymbol{V}}{\mathrm{D}t} = -\nabla p + \boldsymbol{J} \times \boldsymbol{B} + \nu \left(\nabla^2 \boldsymbol{V} + \frac{1}{3} \nabla \left(\nabla \cdot \boldsymbol{V} \right) \right). \tag{4.4}$$

where p is obtained from the equation of state, 4.3.

4.2 Simulation Setup

Simulations were carried out on a domain of dimensions $x \in [-\pi, \pi]$, $ky \in [-\pi, \pi]$, $z = 0$ with periodic boundary conditions. Here, k is the wavenumber of the perturbations to be introduced. The domain size along y was chosen depending on k so that the X-points form right at the boundaries of the simulation domain. Values of viscosity and diffusivity were chosen such that $\nu \sim 10^{-4}$ and $\mu \sim 10^{-3}$, and the density of the plasma, $\rho \sim 1$. This sets the Lundquist number, $S \sim 10^3$, which satisfies the condition $S \gg 1$. The initial velocity was set to zero. The equilibrium vector potential was set as

$$-\psi_0 = A_z = \frac{1}{\cosh^2 x}. \tag{4.5}$$

This choice sets the equilibrium magnetic field and the current density as

$$B_{\perp 0} = -2 \operatorname{sech} x \tanh x, \tag{4.6}$$

$$J_z = \frac{4 \sinh^2 x - 2}{\cosh^4 x}. \tag{4.7}$$

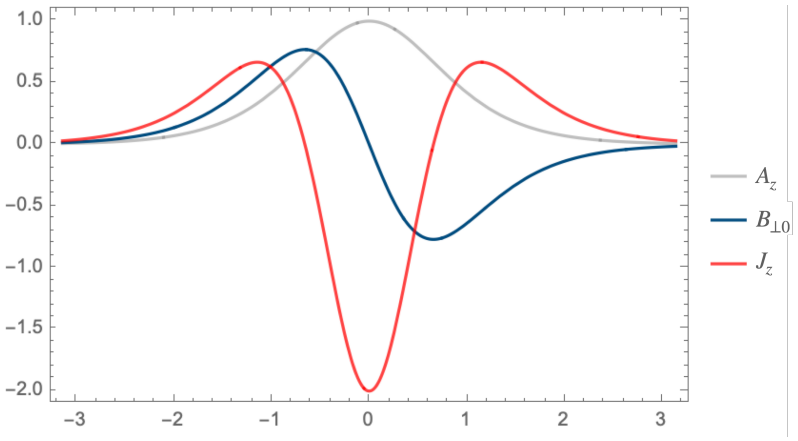

Figure 4.1: Plots of the Equilibrium Fields - A_z, $B_{\perp 0}$ and J_z.

Figure 4.1 shows a plot depicting the equilibrium fields. The existence of a current sheet at $x = 0$ is clear from the figure, as is the reversal of magnetic field as we move across the y-axis.

The instability parameter, Δ', was calculated for this particular form of ψ by substituting $f(x) = \partial_x \left(-\frac{1}{\cosh^2 x} \right)$ in equation 3.8, which reduces to

$$\partial_x^2 \psi_1 - \left(k^2 + 4 - \frac{12}{a^2 \cosh^2 x} \right) \psi_1 = 0. \tag{4.8}$$

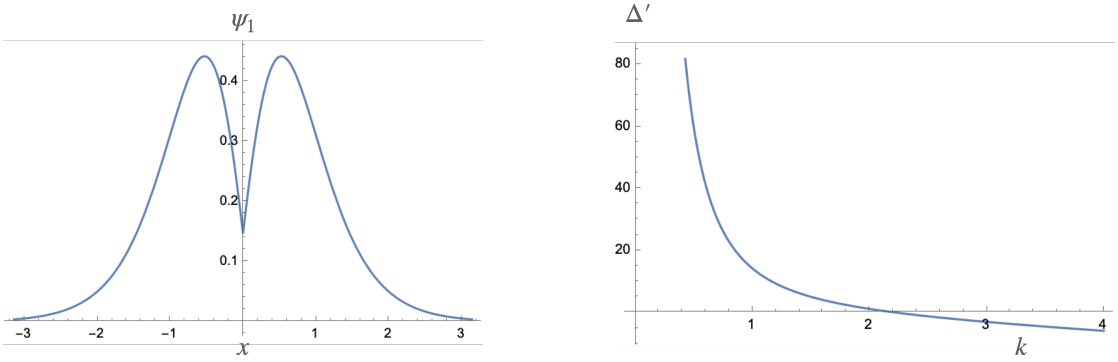

Figure 4.2: *Left:* Plot of ψ_1 vs x as obtained from equation 4.8.
Right: Variation of Δ' with the wave number, k.

Solving the above for ψ_1, we get

$$\psi_1 = \left(\operatorname{sech}^2 x \right)^{k/2} \, {}_2F_1 \left[\frac{k}{2} - \frac{3}{2}, \frac{k}{2} + 2, k + 1, \operatorname{sech}^2(x) \right], \tag{4.9}$$

and subbing this into equation 3.13 yields

$$\Delta' = 2\left[\frac{6k^2+15}{k^2\sqrt{k^2+4}} - \sqrt{k^2+4}\right]. \tag{4.10}$$

Figure 4.2 shows a plot of ψ_1 vs x alongside which the variation of Δ' with k is also shown. As can be seen, Δ' is zero for $k = \sqrt{5}$ and $\Delta' < 0$ for $k > \sqrt{5}$, which means we do not get an instability for $k \geq \sqrt{5}$. Perturbations with $k \in (0, \sqrt{5})$ and relative magnitude of 10^{-4} were introduced and their growth was observed.

4.3 Results

Simulations with $x \times y$ resolutions ranging from 256×256 to 8192×128 were performed for different values of k and η.

The growth of the tearing mode instability was observed. Contour plots of ψ at various times for $k = 1$, $\Delta' = 14.31$ are plotted in figure 4.3 which show an increase in the island width with time. The growth rate, γ, was estimated using two approaches described below.

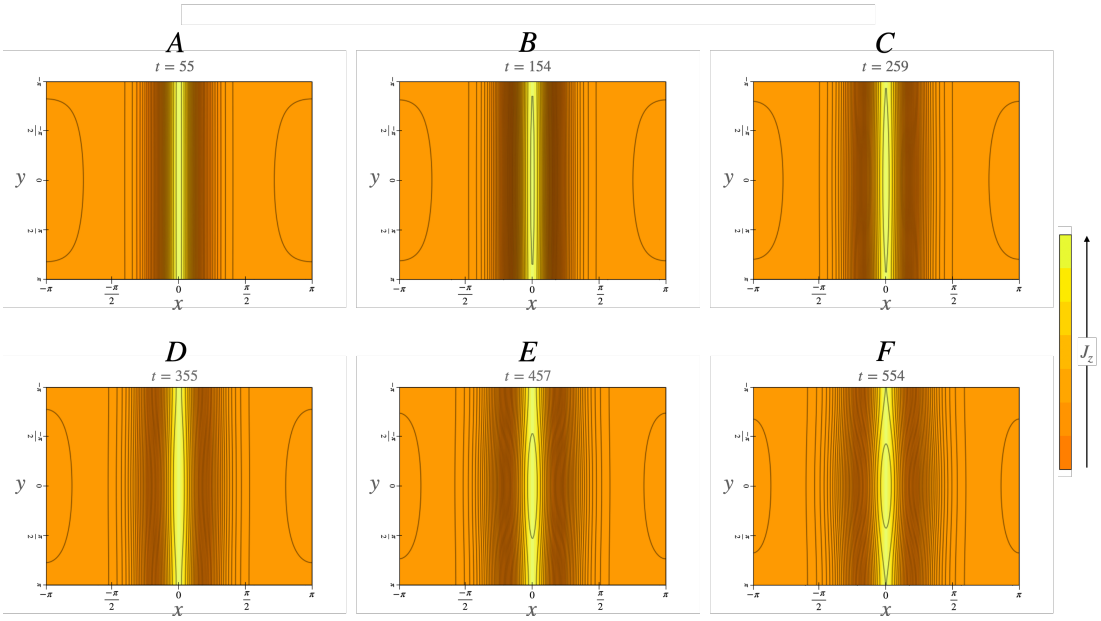

Figure 4.3: Growth of perturbations with time. The perturbations are barely visible in plot A. Plot B shows a recently reconnected island, as does plot C. The growing island width is visible across plots D and E, and plot F shows the location of the X-points - at the boundaries of the domain.

4.3.1 Measuring ψ at an X-point

The first attempt to get γ used values of ψ at any one of the X-points. At an X-point, $\psi(x, y, t) = \psi_0(x) - \psi_1(x)\exp(\gamma t)$ because $ky = \pi$ and so $\cos(ky = \pi) = -1$.Since the perturbation was negligibly small at

$t = 0$, $\psi(0) \approx \psi_0$, which implies $\psi(t) - \psi(0) \approx \psi(t) - \psi_0 = -\psi_1(x)\exp(\gamma t)$. As a result, $\psi(t) - \psi_0$, if known, can be plotted vs time, the resulting curve can be fit to an exponential, and γ can be extracted from the fit.

$\psi(0)$ was supplied by us and Pencil-Code gives us the values of $\psi(t)$ at all points in the domain with a frequency, f_{snap}. Using the values of $\psi(0)$ and $\psi(t)$ at an X-point, $\psi(t) - \psi_0$ vs time was plotted. Figure 4.4 shows one such plot. As can be seen, we did not observe an exponential growth of ψ, instead, we see that the instability growth becomes non-linear at very early times.

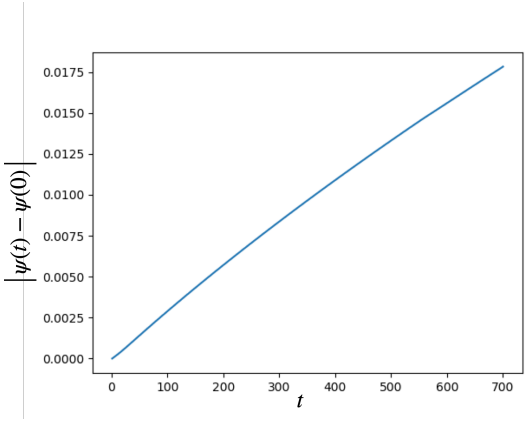

Figure 4.4: $|\psi(t) - \psi(0)|$ vs time - showing non-linear growth right from the beginning.

Further attempts were made to get the linear growth by increasing f_{snap} to finely resolve the initial dynamics and get the linear stage. This resulted in curves which do fit to an exponential however, for reasons not yet understood, the same value for γ was seen for different k values. Two of these curves are shown in figure 4.5.

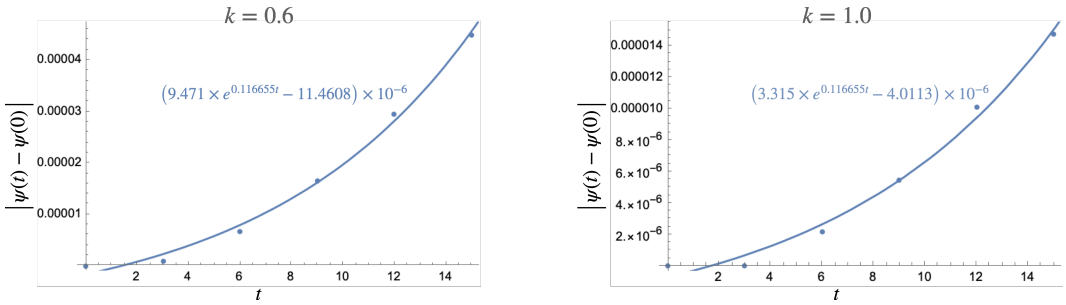

Figure 4.5: $|\psi(t) - \psi(0)|$ vs time - all values of k give $\gamma \sim 0.1166$

4.3.2 Island Width to the Rescue?

The other method we tried out was to measure variation of the island width with time. It can be shown that, theoretically, the island width also increases exponentially. The island width was measured by following a ψ-contour line passing through the X-points and seeing where it intercepts the x-axis. However,

an exponential growth was not seen even for very high spatiotemporal resolutions. A typical plot showing W vs time is shown in figure 4.6

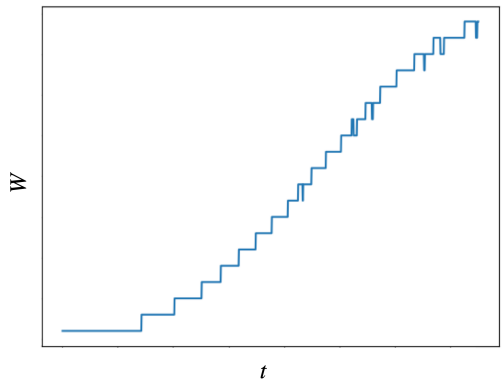

Figure 4.6: Variation of island width with time - also shows non-linear growth from the beginning.

4.4 Discussion

To prevent shocks, Pencil-Code has a lower bound on the diffusivity, η, which was assumed to be small in the derivation of the growth rate for the tearing mode instability. This lower bound, which depends on the resolution of the grid, might be too high for observing the linear growth. Higher the resolution, smaller this lower bound. Multiple attempts were made to obtain the linear stage by increasing the resolution to a maximum of 8192 grid points along the x-axis, the range of which was 2π. Further, all this was attempted for three different forms of the equilibrium fields:

1. $\psi_0 \sim \dfrac{1}{\cosh^2(x)}$,
2. $\psi_0 \sim \ln[\cosh(x)]$,
3. $\psi_0 \sim \sin(x)$.

Despite this, the linear stage of the tearing mode was not observed. At this point, we speculate that sufficiently low values of η to observe the tearing mode instability are unaccessible in Pencil-Code.

Bibliography

[1] Dobler, W., Haugen, N. E., Yousef, T. A., & Brandenburg, A. (2003). Bottleneck effect in three-dimensional turbulence simulations. Physical Review E, 68(2). https://doi.org/10.1103/physreve.68.026304

[2] Furth, H. P., Killeen, J., & Rosenbluth, M. N. (1963). Finite-resistivity instabilities of a sheet pinch. Physics of Fluids, 6(4), 459. https://doi.org/10.1063/1.1706761

[3] Coppi, B., Galvao, R., Pellat, R., Rosenbluth, M. N., & Rutherford, P. M. (1976). Resistive internal kink modes. Soviet Journal of Plasma Physics, 2, 533–535.

[4] Rutherford, P. H. (1973). Nonlinear growth of the tearing mode. Physics of Fluids, 16(11), 1903. https://doi.org/10.1063/1.1694232

[5] The Pencil Code Collaboration, Brandenburg, A., Johansen, A., Bourdin, P., Dobler, W., Lyra, W., Rheinhardt, M., Bingert, S., Haugen, N., Mee, A., Gent, F., Babkovskaia, N., Yang, C.-C., Heinemann, T., Dintrans, B., Mitra, D., Candelaresi, S., Warnecke, J., Käpylä, P., ... Qian, C. (2021). The pencil code, a modular MPI code for partial differential equations and particles: Multipurpose and multiuser-maintained. Journal of Open Source Software, 6(58), 2807. https://doi.org/10.21105/joss.02807